ISSN: 2639-7536

Research Article

Petroleum and Chemical Industry International

Construction and Evaluation of Plasmonic Refractive Index Sensors Based on Dimensional Change and Number of Resonators

Hamid Abbasi*

University of Mazandaran, Iran

***Corresponding Author**
Hamid Abbasi, University of Mazandaran, Iran.

Submitted: 2023, July 15; **Accepted**: 2023, Aug 10: **Published**: 2023, Aug 16

Citation: Abbasi, H. (2023). Construction and Evaluation of Plasmonic Refractive Index Sensors Based on Dimensional Change and Number of Resonators. *Petro Chem Indus Intern, 6*(4), 261-272.

Abstract
In this paper, a plasmonic refractive index sensor based on metal insulated metal waveguide (MIM) with two plasmonic waveguides and five rings and two teeth and four rectangular cavities is proposed and designed. The resonant wavelengths and refractive index of the resonators will be investigated by the time domain finite difference method. To achieve an optical sensor with excellent quality and performance, we change the number and type of amplifiers and their dimensions. In each step of the simulation, we change the refractive index of the middle ring located in the middle of the two waveguides and the refractive index of the other resonators remains constant. This challenge will help to form a more appropriate structure for optical sensors. The sensor built in this simulation has a balanced and suitable function for integrated circuits and helps researchers to better understand the design of plasmonic structures. It also has wide applications in biomedical research, healthcare, pharmaceuticals, environmental monitoring, internal security and battlefield.

Keywords: Plasmonics, Plasmon Surface Polaritons, Metal Insulation Metal Waveguide, Refractive Index Sensor, Cavities, Optical Integrated Circuits.

1. Introduction

Optical sensors are powerful detection and analysis tools that have vast applications in biomedical research, healthcare, pharmaceuticals, environmental monitoring, homeland security, and the battlefield. Optical sensors are also highly sensitive to changes in the refractive index of the environment due to the specific field distribution of resonances [1]. Therefore, these sensors are widely used to measure the refractive index in the chemical, biomedical and food industries. One of the points to consider in optical sensor analysis is that the sensitivity of optical sensors depends greatly on the material and structure of the sensor. Therefore, to further analyze this issue, we can divide optical refractive index sensors into six using plasmonic and photonic structures [2]:

(a) Metal-based propagating plasmonic eigenwave structur [3-12]
(b) Metal -based localized plasmonic eigenmode structures [13-18]
(c) Dielectric-based propagating photonic eigenwave structures [19-26]
(d) Dielectric-based localized photonic eigenmode structures [27-32] (e) Advanced hybrid structures [33-38] (f) 2D material integrated structures [39-42].

In this paper, we consider the first case, a metal-based plasmonic sensor built on a specific plasmonic wave, the superficial plasmon polariton (SPP). SPP is a non-radiative electromagnetic surface wave that propagates in a direction parallel to the metal-dielectric interface [43-47]. Because the wave is at the boundary between the conductor and the external environment (for example, air or water), these oscillations are very sensitive to any change in this boundary, such as the adsorption of molecules to the conductive surface. Their outstanding ability to overcome the limitations of classical optical diffraction has made SPPs attractive as carriers of energy and information in fully integrated circuits and optical devices. Among the various SPP structures, Insulation-Insulation-Metal (IMI) structures and Metal-InsulationMetal (MIM) structures are two important plasmonic multilayer structures. Due to the support modes with deep sub-wavelength scales, high bandwidth in a very wide range of frequencies, very high optical confinement and acceptable propagation length [48], we choose Metal Insulation Metal (MIM). Metal-insulator-metal (MIM) structuresو such as optical filters [4952], optical switches [53], demultiplexers [54,55] and sensors [56-59], are widely used. also Plasmonic sensors based on MIM waveguide structures, such as asymmetric nanodisk filter and sensor [60–62], side-coupled cavity sensor [63], notch resonator filter and sensor [64], and circular ring filter and sensor [65,66], are one of the most important optical devices, have attracted tremendous attention, and have been investigated widely in recent years. Therefore, in this study, we begin to design and build a plasmonic sensor consisting of arrays of metal insulated metal waveguides (MIM) and plasmonic resonators.

2. Drawing the Structure of the Plasmonic Sensor and Analysing its Structural Model

The structure of our proposed sensor consists of two plasmonic waveguides, five rings, two teeth and four rectangular cavities (Fig.1). The two waveguides have a height of W_1 = 50 nm. The middle ring, which is located in the middle of two waveguides, has an inner radius of r_1 = 90 nm and an outer radius of R_1 = 125 nm. Also, two tooth are connected to the middle ring, which has a height of 20 nm and a length of 40 nm. Four rings with equal inner radius and outer radius are located in the upper and lower parts of the waveguides, which have inner radius $r_2 = r_3 = r_4 = r_5$ = 91 nm and outer radius $R_2 = R_3 = R_4 = R_5$ = 126 nm, respectively. The two monitors P_{in} and P_{out} are input and output monitors, respectively, which are used to measure the input and output waves. The wave transmission is calculated by the following equation:

$$T = P_{out} / P_{in} \qquad (1)$$

Also, the simulation substrate is made of silver metal and the waveguides and amplifiers are made of air. To show the optical properties of metals in simulation, we use the greeting model:

$$\varepsilon)\omega(= \varepsilon_\infty - \omega p^2 / \omega^2 + i\Upsilon\omega \qquad (2)$$

Here ε_∞ =1 gives the medium constant for the infinite frequency, ωp = 1.37 × 1016 refers to bulk frequency for plasma, γ = 3.21 × 1013 means damping frequency for electron oscillation, and ω shows incident light angular frequency.

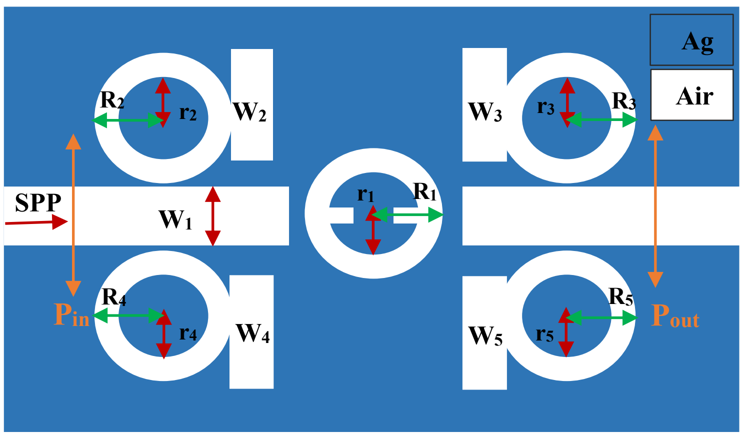

Figure 1: Two-dimensional image of a plasmonic sensor

Because the height of the waveguides is smaller than the wavelength of the radiated light, only the TM mode can exist in the sensor structure and participate in the simulation. The TM wave starts moving from the left and goes through the left waveguide to the resonators. Each resonators reflects or allows a portion of the input wave signal to pass through. Eventually the wave reaches the output waveguide, the intensity of which decreases at the end of the path relative to the beginning of its motion. To explain the electric field distribution, it can be said that when the field distribution in structures is equal and similar, energy loss is reduced. Therefore, in order to achieve the maximum field distribution in the sensor structure, all dimensions must be optimal.

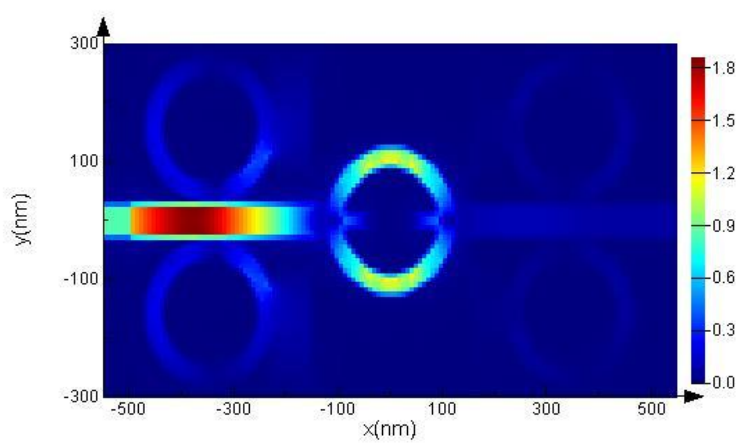

Figure 2: Plasmonic sensor field distribution

3. Sensor Design Methods Using the Field-Limited Difference Method and Refractive Index Measurement.

Using the time domain finite difference method, we examine and analyze the sensor performance (numerical analysis) and using the transmission line model method, we theoretically examine the performance of the sensor. Summarizing these two methods, we analyze the proposed structure resonance behavior and get a functional plasmonic sensor. For the numerical approach, we use the finite difference method of time domain and boundary condition with perfectly matched PML layers. We consider the mesh size to be 8 nm for both x and y directions. To reduce the simulation time and create a suitable space, we do the simulation in two dimensions. To measure the performance of the sensor and to technically test the designed structure, we examine each of the cavities separately, and in the last step, we examine all the components of the structure as shown in Fig.1. That is, first we analyze this sensor in detail and then in general.

4. Simulation and Design of the Sensor Using Two Waveguides and a Ring With Two Tooth.

In the first stage, only the middle ring and its two teeth are present, which are placed in the middle of two plasmonic waveguides (Fig.3).

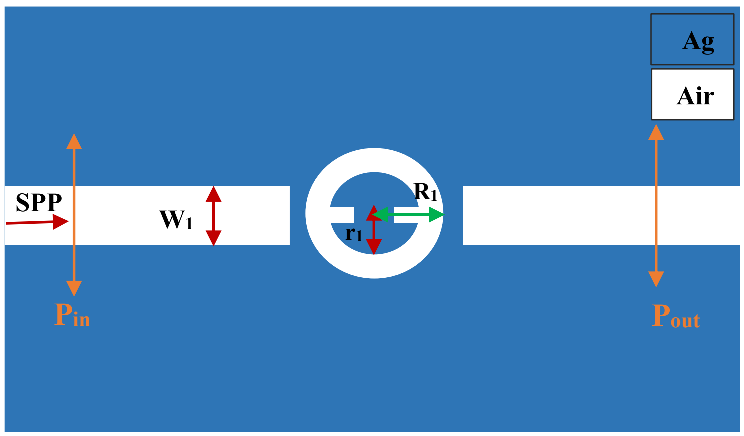

Figure 3: Two-dimensional image of a plasmonic sensor

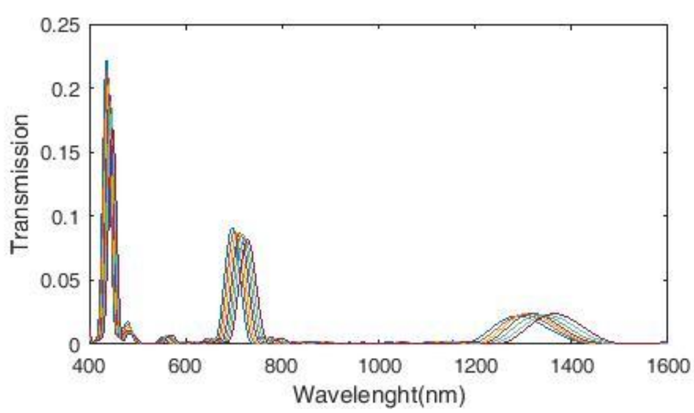

Figure 4: Transmission spectrum of plasmonic refractive index sensor with one ring and two tooth

We change the refractive index of the middle ring by a step of 0.01 from 1.14 to 1.2, which leads to a change in the spectra and the wavelength of the resonance. The first characteristic that must be calculated to measure the performance of a sensor is the sensitivity of S: $S = \Delta\lambda / \Delta n$ (nm / RIU) (3).

In this equation, $\Delta\lambda$ is the change in resonance wavelength, Δn is the change in refractive index. The graph of the sensitivity coefficient of a plasmonic sensor is shown in Fig.5. According to the figure, the maximum sensitivity for the refractive index is n = 1. 2 (in mode 3), which is equal to 1298 nm / RIU.

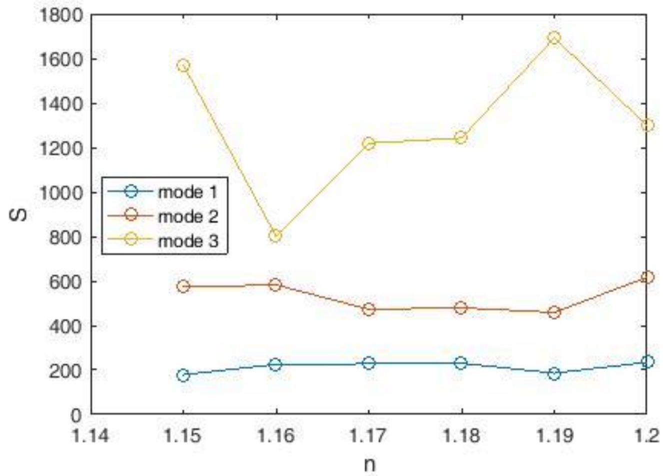

Figure 5: Plasmonic sensor sensitivity coefficient diagram with a ring and two teeth

Next, we calculate and examine the figure of merit (FOM). The obtained diagram (Fig.6) along with the S-sensitivity coefficient diagram will help us to achieve a quality sensor: FOM = S / FWHM (4)

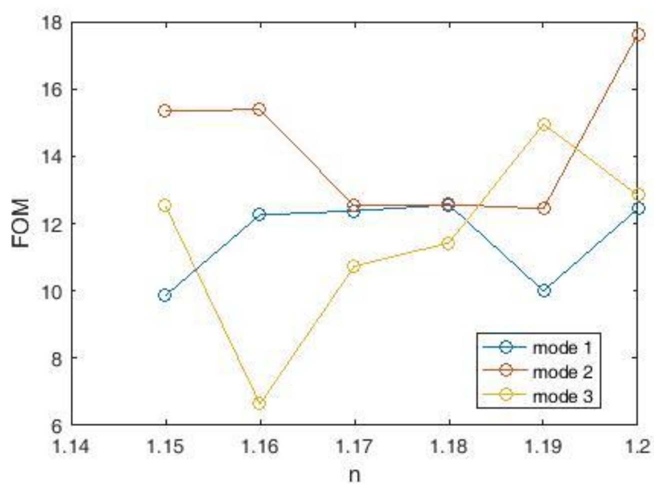

Figure 6: the figure of merit (FOM) Diagram of Plasmonic Sensor.

According to Fig.6, the maximum the figure of merit (FOM) for the refractive index is n = 1.2 (in mode2), which is equal to 17.629 nm / RIU. The last criterion for measuring the designed sensor is Q quality factor: $Q = \lambda_{res} / FWHM$ (5)

According to Fig.7, the maximum value of the quality factor Q is for the refractive index n = 1.15 (in mode1), which is equal to 24.124 nm / RIU.

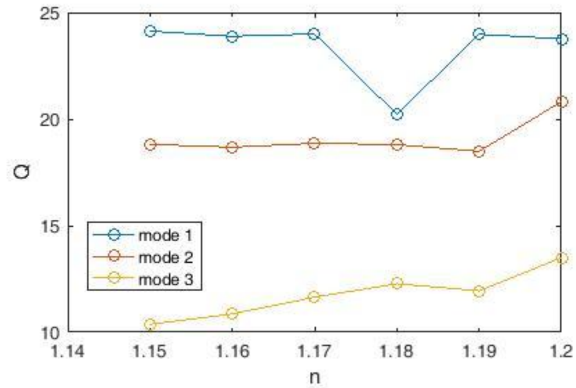

Figure 7: Q-quality coefficient diagram of plasmonic sensor

5. Simulation and Design of The Sensor Using Two Waveguides and Five Rings With Two Tooth

In this step, we add four rings to the middle ring and its two tooth (Fig.8) and seek to increase the performance of the proposed sensor by increasing the number of cavities and changing their coordinates.

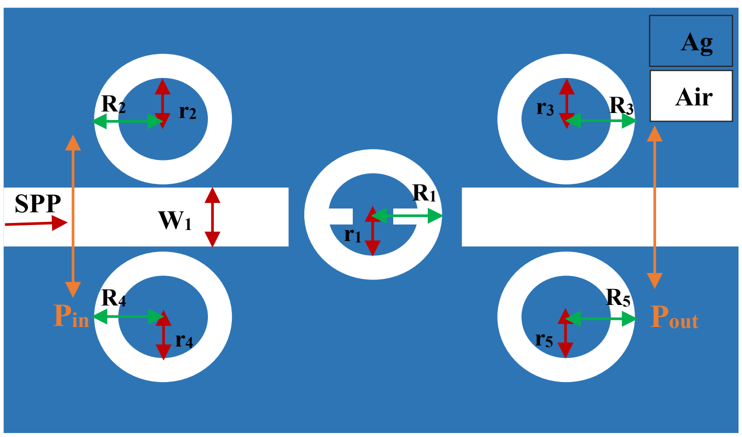

Figure 8: Two-dimensional image of a plasmonic sensor

We see the transmission spectrum of the designed sensor device in Fig.9. The transmission spectrum has three peaks. The left peak has a narrower FWHM and the right peak has a wider FWHM. The middle peak has the highest height. But the right peak will perform better than the other two peaks because it has the highest amount of wavelength change per refractive index change.

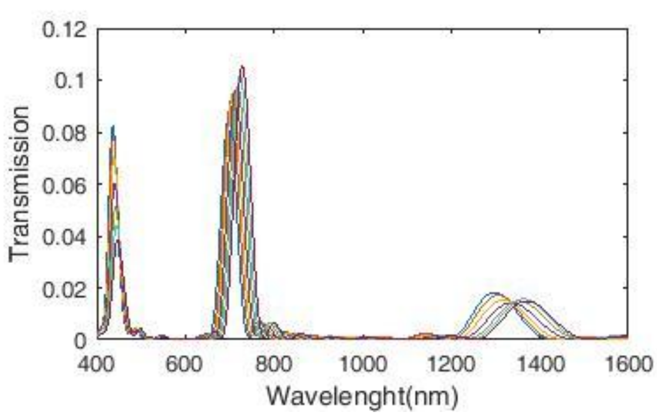

Figure 9: Transmission spectrum of plasmonic refractive index sensor with five rings and two tooth

Now we change the refractive index of the middle ring with a step of 0.01 from 1.14 to 1.2 and calculate the sensitivity of the sensor, which according to Figure 10 has the highest sensitivity for the refractive index n = 1.18 (in mode 3), which is equal to 1692 nm / RIU.

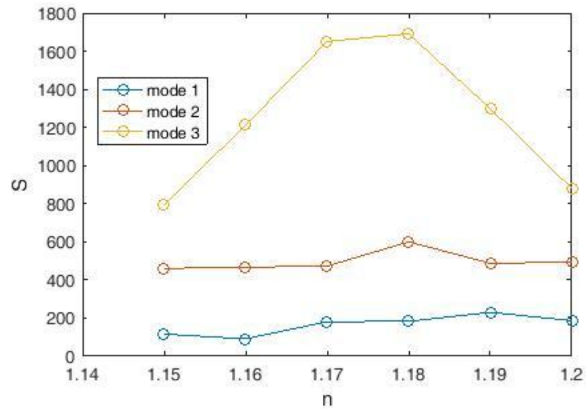

Figure 10: Sensitivity coefficient diagram of a plasmonic refractive index sensor with five rings and two tooth.

Next, we calculate the figure of merit (FOM) and the Q quality factor and draw diagrams for them (Fig.11). According to the figure, the highest figure of merit (FOM) for the refractive index is n = 1.18 (in mode2), which is equal to 14.168 nm/RIU and the highest quality coefficient Q for refractive index n = 1.18 (in mode1) which is equal to 19.994 nm / RIU.

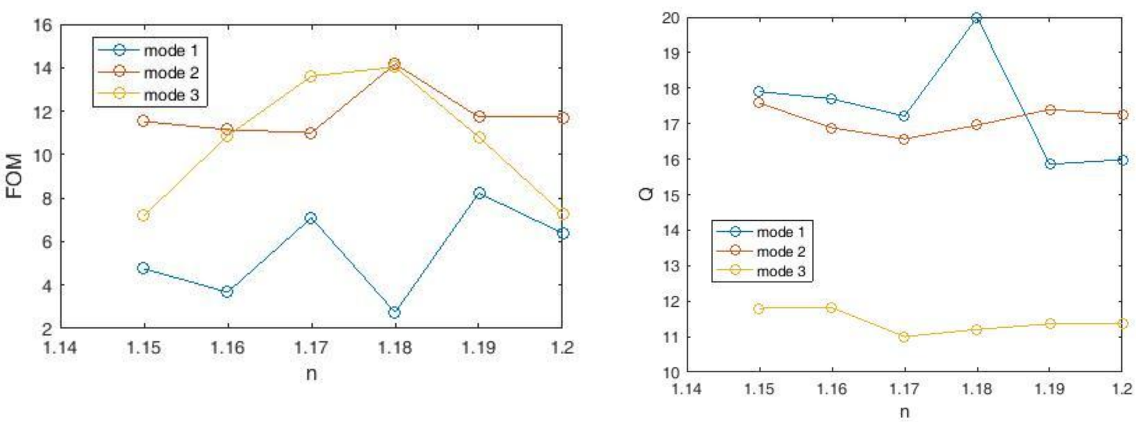

Figure 11: Diagram of figure of merit (FOM) and quality coefficient diagram of Q plasmonic sensor with five rings and two tooth.

6 .Simulation and Design of The Sensor Using Two Waveguides and Four Cavities and a Ring With Two Tooth

At this stage of the simulation, there are four cavities and a middle ring and two tooth (Fig.12).

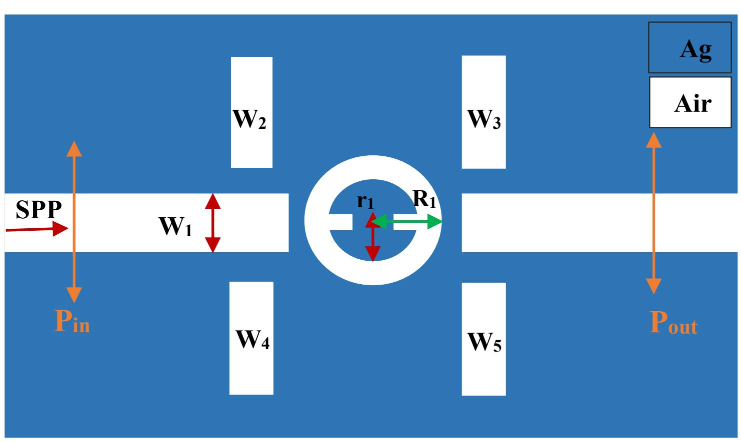

Figure 12: Two-dimensional image of a plasmonic sensor

We see the transmission spectrum of the designed sensor device in Fig.13. The transmission spectrum has three peaks. As in the previous sensor structure (Fig.9), the left peak has a narrower FWHM and the courier on the right has a wider FWHM. But a change has been made compared to the previous structure and the highest height belongs to the left peak. But again, the right peak will perform better than the other two peaks because it has the highest amount of wavelength change per refractive index change.

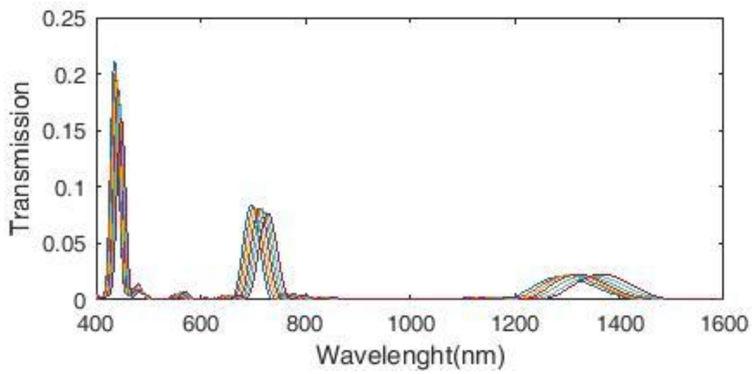

Figure 13: Transmission spectrum of plasmonic refractive index sensor with a ring, two tooth and four cavities

Now we change the refractive index of the middle ring with a step of 0.01 from 1.14 to 1.2 and calculate the sensitivity of the sensor, which according to Figure 10 has the highest sensitivity for the refractive index n = 1.19 (in mode 3), which is equal to 1692 nm / RIU.

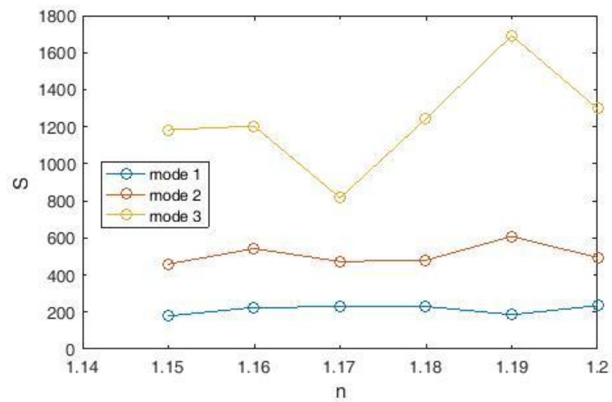

Figure 14: Sensitivity coefficient diagram of a plasmonic refractive index sensor with a ring, two tooth and four cavities.

We calculate the figure of merit (FOM) and the Q quality factor and we will draw diagrams for them (Fig.15). According to the figure, the highest fitness figure of merit (FOM) for the refractive index is n = 1.16 (in mode2), which is equal to 14.475 nm / RIU, which has a higher FOM value than the previous structure (Fig.11). Also, the highest quality factor Q for the refractive index is n = 1.18 (in mode1), which is equal to 23.99 nm / RIU, which has a higher value of Q than the previous structure (Fig.11).

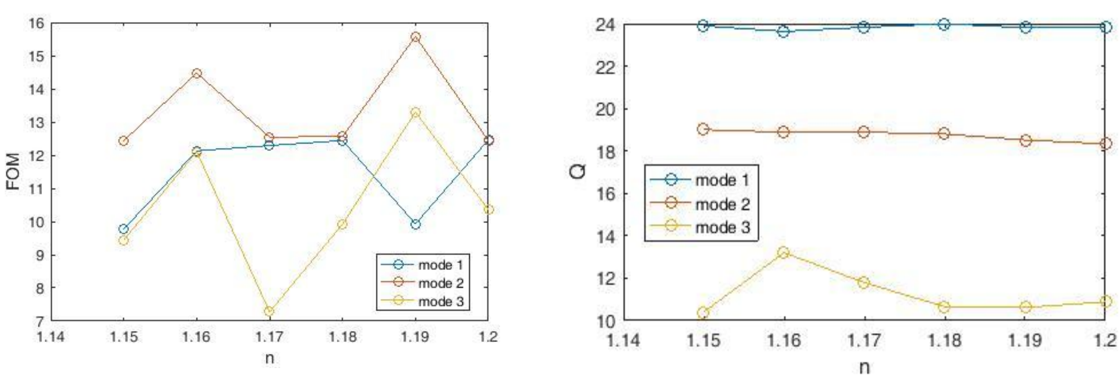

Figure 15: Diagram of figure of merit (FOM) and Q coefficient diagram of plasmonic sensor with a ring, two tooth and four cavities.

7 . Simulation and Design of the Sensor Using Two Waveguides and Four Cavities and Five Rings With Two Tooth

In this step of the simulation, we design a plasmonic sensor whose structure is the sum of the two structures of Figures 8 and 12. To use it to reach a general conclusion about the sensor we want. The structure of this sensor will include two waveguides, four cavities and five rings and two tooth (Figure 16).

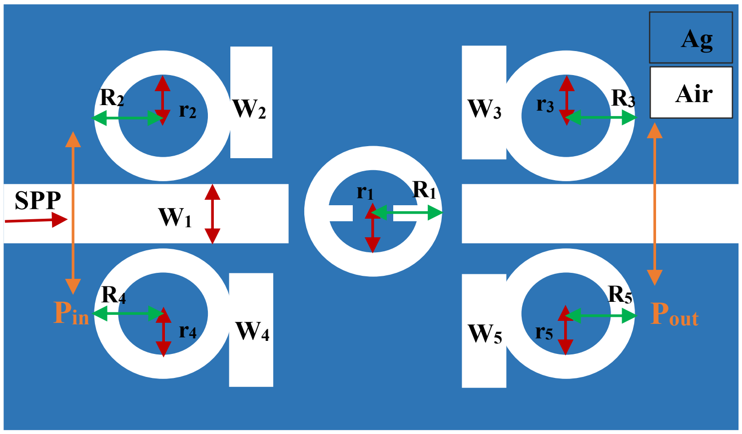

Figure 16: Two-dimensional image of a plasmonic sensor

We see the transmission spectrum of the designed sensor device in Fig.17. The transmission spectrum has two peaks. The courier on the left has a narrower FWHM and the courier on the right has a wider FWHM. The highest height belongs to the peak on the left. But the right peak will perform better than the other peak because it has the highest amount of wavelength change per refractive index change.

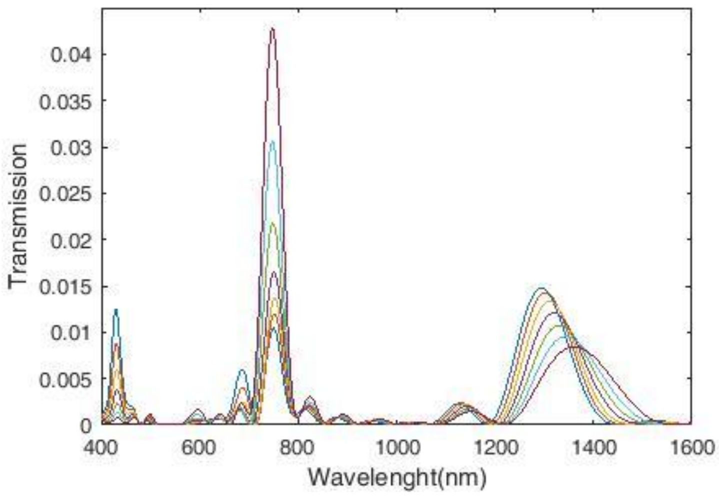

Figure 17: Plasmonic refractive index sensor transmission spectrum with four cavities, five rings and two tooth.

Now change the refractive index of the middle ring by step 0.01 nm from 1.14 to 1.2 and we calculate the sensitivity of the sensor, which according to Fig.18 has the highest sensitivity for the refractive index n = 1.2 (in mode2), which is equal to 1714 nm / RIU.

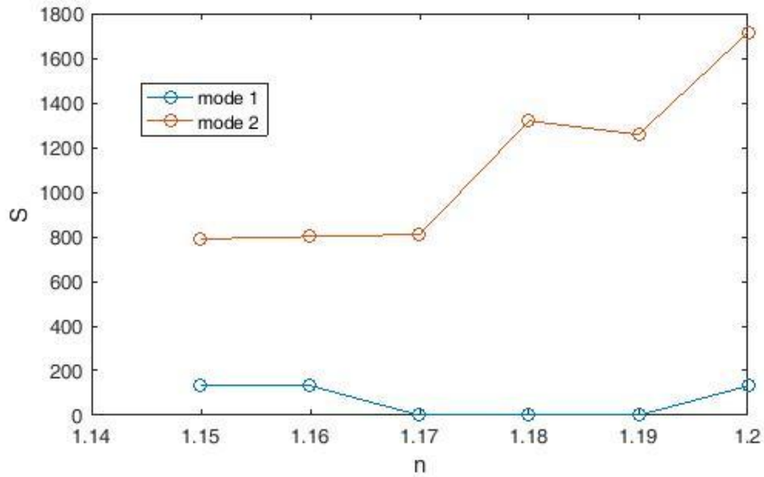

Figure 18: Sensitivity coefficient diagram of a plasmonic refractive index sensor with four cavities, five rings and two tooth.

We calculate the figure of merit (FOM) and the Q quality factor and we will draw diagrams for them (Fig.19). According to the figure, the highest competence figure (FOM) for the refractive index is n = 1.2 (in mode2), which is equal to 10.407 nm / RIU. Also, the highest quality factor Q is for the refractive index n = 1.15 (in mode1), which is equal to 19.55 nm / RIU.

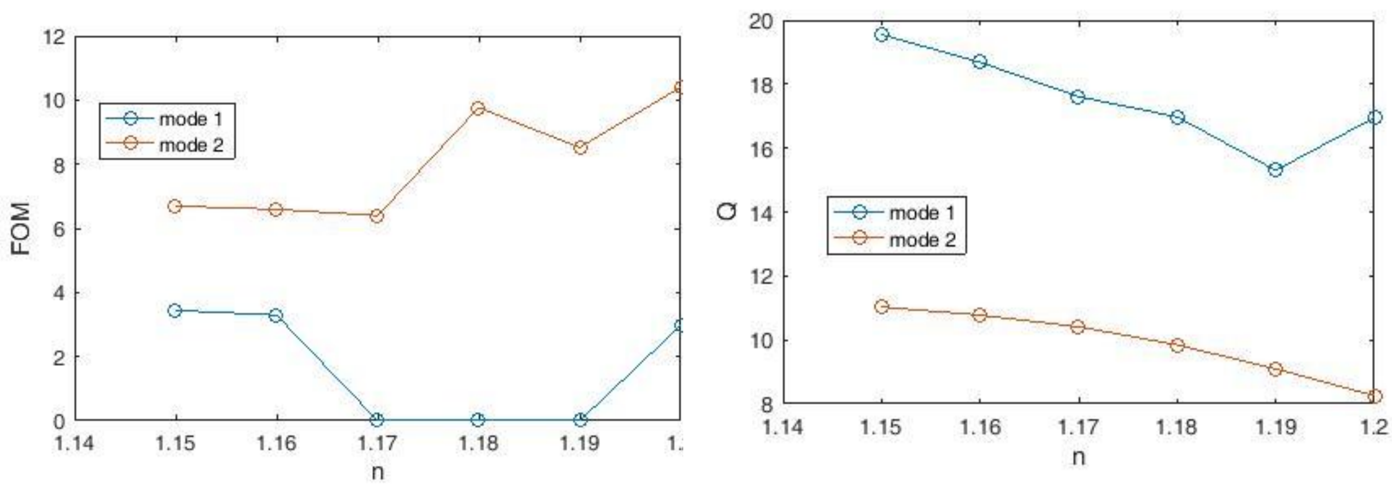

Figure 19: Diagram of competency figure (FOM) and quality coefficient diagram of Q plasmonic sensor with four cavities, five rings and two tooth.

8. Conclusion

Refractive index sensors are divided into six categories based on structure (plasmonic and photonic). The dimensions and coordinates of the sensor structure have a great effect on increasing the sensor performance. In this paper, we evaluate sensor performance by changing the coordinates and structure of the sensor, as well as changing the refractive index of the resonators. The resonant wavelength spectrum will change evenly, helping to better design the sensor. Due to its small size and balanced performance, this configuration is suitable for use in fully integrated circuits.

Competing Interest

The authors declare no conflicts of interest.

Data Availability

The data that support the findings of this study are available from the corresponding author upon reasonable request.

Reference

1. Santos, D., Temperini, M., Brolo, A. E., Szunerits, S., & Boukherroub, R. (2015). Introduction to Plasmonics.
2. Xu, Y., Bai, P., Zhou, X., Akimov, Y., Png, C. E., Ang, L. K., ... & Wu, L. (2019). Optical refractive index sensors with plasmonic and photonic structures: promising and inconvenient truth. Advanced Optical Materials, 7(9), 1801433.A. Shalabney, I. Abdulhalim, Opt. Lett. 2012, 37, 1175.
3. Dostálek, J., Vaisocherová, H., & Homola, J. (2005).

Multichannel surface plasmon resonance biosensor with wavelength division multiplexing. Sensors and Actuators B: Chemical, 108(1-2), 758-764.
4. Nair, S., Escobedo, C., & Sabat, R. G. (2017). Crossed surface relief gratings as nano plasmonic biosensors. ACS sensors, 2(3), 379-385.
5. Liu, Z., Wei, Y., Zhang, Y., Zhang, Y., Zhao, E., Yang, J., & Yuan, L. (2015). Twin-core fibre SPR sensor. Optics Letters, 40(12), 2826-2829.
6. Liu, Z., Wei, Y., Zhang, Y., Wang, Y., Zhao, E., Zhang, Y., ... & Yuan, L. (2016). A multi-channel fibre SPR sensor based on TDM technology. Sensors and Actuators B: Chemical, 226, 326-331.
7. Baiad, M. D., & Kashyap, R. (2015). Concatenation of surface plasmon resonance sensors in a single optical fiber using tilted fiber Bragg gratings. Optics Letters, 40(1), 115-118.
8. Caucheteur, C., Shevchenko, Y., Shao, L. Y., Wuilpart, M., & Albert, J. (2011). High resolution interrogation of tilted fiber grating SPR sensors from polarization properties measurement. Optics express, 19(2), 1656-1664.
9. Renoirt, J. M., Debliquy, M., Albert, J., Ianoul, A., & Caucheteur, C. (2014). Surface plasmon resonances in oriented silver nanowire coatings on optical fibers. The Journal of Physical Chemistry C, 118(20), 11035-11042.
10. Renoirt, J. M., Debliquy, M., Albert, J., Ianoul, A., & Caucheteur, C. (2014). Surface plasmon resonances in oriented silver nanowire coatings on optical fibers. The Journal of Physical Chemistry C, 118(20), 11035-11042.
11. Bolduc, O. R., Live, L. S., & Masson, J. F. (2009). High-resolution surface plasmon resonance sensors based on a dove prism. Talanta, 77(5), 1680-1687.
12. Chen, H., Kou, X., Yang, Z., Ni, W., & Wang, J. (2008). Shape-and size-dependent refractive index sensitivity of gold nanoparticles. Langmuir, 24(10), 5233-5237.
13. Khan, A. U., Zhao, S., & Liu, G. (2016). Key parameter controlling the sensitivity of plasmonic metal nanoparticles: aspect ratio. The Journal of Physical Chemistry C, 120(34), 19353-19364.
14. Gartia, M. R., Hsiao, A., Pokhriyal, A., Seo, S., Kulsharova, G., Cunningham, B. T., ... & Liu, G. L. (2013). Colorimetric plasmon resonance imaging using nano lycurgus cup arrays. Advanced Optical Materials, 1(1), 68-76.
15. Chang, T. W., Wang, X., Hsiao, A., Xu, Z., Lin, G., Gartia, M. R., ... & Liu, G. L. (2015). Bifunctional Nano Lycurgus Cup Array Plasmonic Sensor for Colorimetric Sensing and Surface-Enhanced Raman Spectroscopy. Advanced Optical Materials, 3(10), 1397-1404.
16. Li, Q., Zhuo, X., Li, S., Ruan, Q., Xu, Q. H., & Wang, J. (2015). Production of monodisperse gold nanobipyramids with number percentages approaching 100% and evaluation of their plasmonic properties. Advanced Optical Materials, 3(6), 801-812.
17. Lodewijks, K., Van Roy, W., Borghs, G., Lagae, L., & Van Dorpe, P. (2012). Boosting the figure-of-merit of LSPR-based refractive index sensing by phase-sensitive measurements. Nano letters, 12(3), 1655-1659.
18. Guo, Y., Ye, J. Y., Divin, C., Huang, B., Thomas, T. P., Baker, Jr, J. R., & Norris, T. B. (2010). Real-time biomolecular binding detection using a sensitive photonic crystal biosensor. Analytical chemistry, 82(12), 5211-5218.
19. Liu, T., Liang, L. L., Xiao, P., Sun, L. P., Huang, Y. Y., Ran, Y., ... & Guan, B. O. (2018). A label-free cardiac biomarker immunosensor based on phase-shifted microfiber Bragg grating. Biosensors and Bioelectronics, 100, 155-160.
20. Guo, T., Liu, F., Liu, Y., Chen, N. K., Guan, B. O., & Albert, J. (2014). In-situ detection of density alteration in non-physiological cells with polarimetric tilted fiber grating sensors. Biosensors and Bioelectronics, 55, 452-458.
21. Jiang, B., Zhou, K., Wang, C., Sun, Q., Yin, G., Tai, Z., ... & Zhang, L. (2018). Label-free glucose biosensor based on enzymatic graphene oxide-functionalized tilted fiber grating. Sensors and Actuators B: Chemical, 254, 1033-1039.
22. Coelho, L., Viegas, D., Santos, J. L., & De Almeida, J. M. M. M. (2016). Characterization of zinc oxide coated optical fiber long period gratings with improved refractive index sensing properties. Sensors and Actuators B: Chemical, 223, 45-51.
23. Jia, P., Fang, G., Liang, T., Hong, Y., Tan, Q., Chen, X., ... & Xiong, J. (2017). Temperature-compensated fiber-optic Fabry–Perot interferometric gas refractive-index sensor based on hollow silica tube for high-temperature application. Sensors and Actuators B: Chemical, 244, 226-232.
24. Farmer, A., Friedli, A. C., Wright, S. M., & Robertson, W. M. (2012). Biosensing using surface electromagnetic waves in photonic band gap multilayers. Sensors and Actuators B: Chemical, 173, 79-84.
25. Sinibaldi, A., Danz, N., Descrovi, E., Munzert, P., Schulz, U., Sonntag, F., ... & Michelotti, F. (2012). Direct comparison of the performance of Bloch surface wave and surface plasmon polariton sensors. Sensors and Actuators B: Chemical, 174, 292-298.
26. Fegadolli, W. S., Pavarelli, N., O'Brien, P., Njoroge, S., Almeida, V. R., & Scherer, A. (2015). Thermally controllable silicon photonic crystal nanobeam cavity without surface cladding for sensing applications. ACS Photonics, 2(4), 470-474.
27. Abbasi, H. (2022). Construction and Evaluation of Plasmonic Refractive Index Sensor Based on Changing the Number of Resonators and Changing Their Dimensions.
28. Chandran, S., Gupta, R. K., & Das, B. K. (2016). Dispersion enhanced critically coupled ring resonator for wide range refractive index sensing. IEEE Journal of Selected Topics in Quantum Electronics, 23(2), 424-432.
29. Caër, C., Serna-Otálvaro, S. F., Zhang, W., Le Roux, X., & Cassan, E. (2014). Liquid sensor based on high-Q slot photonic crystal cavity in silicon-on-insulator configuration. Optics letters, 39(20), 5792-5794.
30. Xu, X., Subbaraman, H., Chakravarty, S., Hosseini, A., Covey, J., Yu, Y., ... & Chen, R. T. (2014). Flexible single-crystal silicon nanomembrane photonic crystal cavity. Acs Nano, 8(12), 12265-12271.

31. Bao, Y., Hu, Z., Li, Z., Zhu, X., & Fang, Z. (2015). Magnetic plasmonic Fano resonance at optical frequency. Small, 11(18), 2177-2181.K. L. Lee, J. B. Huang, J. W. Chang, S. H. Wu, P. K. Wei, Sci. Rep. 2015, 5, 8547.
32. Lodewijks, K., Ryken, J., Van Roy, W., Borghs, G., Lagae, L., & Van Dorpe, P. (2013). Tuning the Fano resonance between localized and propagating surface plasmon resonances for refractive index sensing applications. Plasmonics, 8, 1379-1385.
33. Wang, Y., Wu, L., Wong, T. I., Bauch, M., Zhang, Q., Zhang, J., ... & Liedberg, B. (2016). Directional fluorescence emission co-enhanced by localized and propagating surface plasmons for biosensing. Nanoscale, 8(15), 8008-8016.
34. Baaske, M. D., Foreman, M. R., & Vollmer, F. (2014). Single-molecule nucleic acid interactions monitored on a label-free microcavity biosensor platform. Nature nanotechnology, 9(11), 933-939.
35. Dantham, V. R., Holler, S., Barbre, C., Keng, D., Kolchenko, V., & Arnold, S. (2013). Label-free detection of single protein using a nanoplasmonic-photonic hybrid microcavity. Nano letters, 13(7), 3347-3351.
36. Kravets, V. G., Jalil, R., Kim, Y. J., Ansell, D., Aznakayeva, D. E., Thackray, B., ... & Grigorenko, A. N. (2014). Graphene-protected copper and silver plasmonics. Scientific reports, 4(1), 5517.
37. Zhang, C., Li, Z., Jiang, S. Z., Li, C. H., Xu, S. C., Yu, J., ... & Man, B. Y. (2017). U-bent fiber optic SPR sensor based on graphene/AgNPs. Sensors and Actuators B: Chemical, 251, 127-133.
38. Reed, J. C., Zhu, H., Zhu, A. Y., Li, C., & Cubukcu, E. (2012). Graphene-enabled silver nanoantenna sensors. Nano letters, 12(8), 4090-4094.
39. Liu, C., Cai, Q., Xu, B., Zhu, W., Zhang, L., Zhao, J., & Chen, X. (2017). Graphene oxide functionalized long period grating for ultrasensitive label-free immunosensing. Biosensors and Bioelectronics, 94, 200-206.
40. Barnes, W. L., Dereux, A., & Ebbesen, T. W. (2003). Surface plasmon subwavelength optics. nature, 424(6950), 824-830.
41. Genet, C., & Ebbesen, T. W. (2007). Light in tiny holes. Nature, 445(7123), 39-46.
42. Neutens, P., Van Dorpe, P., De Vlaminck, I., Lagae, L., & Borghs, G. (2009). Electrical detection of confined gap plasmons in metal–insulator–metal waveguides. Nature Photonics, 3(5), 283-286.
43. Gramotnev, D. K., & Bozhevolnyi, S. I. (2010). Plasmonics beyond the diffraction limit. Nature photonics, 4(2), 83-91.
44. Liu, D., Wang, J., Zhang, F., Pan, Y., Lu, J., & Ni, X. (2017). Tunable plasmonic band-pass filter with dual side-coupled circular ring resonators. Sensors, 17(3), 585.
45. Liu, D., Sun, Y., Fan, Q., Mei, M., Wang, J., Pan, Y. W., & Lu, J. (2016). Tunable plasmonically induced transparency with asymmetric multi-rectangle resonators. Plasmonics, 11, 1621-1628.
46. Lin, X. S., & Huang, X. G. (2008). Tooth-shaped plasmonic waveguide filters with nanometeric sizes. Optics letters, 33(23), 2874-2876.
47. Lee, T. W., & Kwon, S. H. (2015). Dual-function metal–insulator–metal plasmonic optical filter. IEEE Photonics Journal, 7(1), 1-8.
48. Zand, I., Bahramipanah, M., Abrishamian, M. S., & Liu, J. M. (2012). Metal–insulator–metal nanoscale loop–stub structures. IEEE Photonics Journal, 4(6), 2136-2142.
49. Lu, H., Liu, X., Mao, D., Wang, L., & Gong, Y. (2010). Tunable band-pass plasmonic waveguide filters with nanodisk resonators. Optics Express, 18(17), 17922-17927.
50. Tao, J., Wang, Q. J., & Huang, X. G. (2011). All-optical plasmonic switches based on coupled nano-disk cavity structures containing nonlinear material. Plasmonics, 6, 753-759.
51. Liu, H., Gao, Y., Zhu, B., Ren, G., & Jian, S. (2015). A T-shaped high resolution plasmonic demultiplexer based on perturbations of two nanoresonators. Optics Communications, 334, 164-169.
52. Wang, G., Lu, H., Liu, X., Mao, D., & Duan, L. (2011). Tunable multi-channel wavelength demultiplexer based on MIM plasmonic nanodisk resonators at telecommunication regime. Optics Express, 19(4), 3513-3518.
53. Wu, T., Liu, Y., Yu, Z., Peng, Y., Shu, C., & Ye, H. (2014). The sensing characteristics of plasmonic waveguide with a ring resonator. Optics express, 22(7), 7669-7677.
54. Lin, Q., Zhai, X., Wang, L. L., Luo, X., Liu, G. D., Liu, J. P., & Xia, S. X. (2016). A novel design of plasmon-induced absorption sensor. Applied Physics Express, 9(6), 062002.
55. Qu, S., Song, C., Xia, X., Liang, X., Tang, B., Hu, Z. D., & Wang, J. (2016). Detuned plasmonic Bragg grating sensor based on a defect metal-insulator-metal waveguide. Sensors, 16(6), 784.
56. Qian, Q., Liang, Y., Liang, Y., Shao, H., Zhang, M., Xiao, T., & Wang, J. (2016). Tunable multiple-step plasmonic Bragg reflectors with graphene-based modulated grating. Sensors, 16(12), 2039.
57. Zhan, G., Liang, R., Liang, H., Luo, J., & Zhao, R. (2014). Asymmetric band-pass plasmonic nanodisk filter with mode inhibition and spectrally splitting capabilities. Optics express, 22(8), 9912-9919.
58. Lu, H., Liu, X., & Mao, D. (2012). Plasmonic analog of electromagnetically induced transparency in multi-nanoresonator-coupled waveguide systems. Physical Review A, 85(5), 053803.
59. Wei, W., Zhang, X., & Ren, X. (2015). Plasmonic circular resonators for refractive index sensors and filters. Nanoscale Research Letters, 10, 1-6.
60. Xie, Y. Y., Huang, Y. X., Zhao, W. L., Xu, W. H., & He, C. (2015). A novel plasmonic sensor based on metal–insulator–metal waveguide with side-coupled hexagonal cavity. IEEE Photonics Journal, 7(2), 1-12.
61. Bahramipanah, M., Abrishamian, M. S., Mirtaheri, S. A., & Liu, J. M. (2014). Ultracompact plasmonic loop–stub notch filter and sensor. Sensors and Actuators B: Chemical, 194, 311-318.

62. Zou, S., Wang, F., Liang, R., Xiao, L., & Hu, M. (2014). A nanoscale refractive index sensor based on asymmetric plasmonic waveguide with a ring resonator: A review. IEEE Sensors Journal, 15(2), 646-650.

63. Zhang, H., Shen, D., & Zhang, Y. (2014). Circular split-ring core resonators used in nanoscale metal–insulator–metal band-stop filters. Laser Physics Letters, 11(11), 115902.